Freeze-Drying Enabled Porous Layered δ-MnO_2/rGO Composite Selected from MnO_2 Polymorphs for High-Performance AZIBs

Jiaoyuan Lu, Xiaojun Tang, Huiting Bi*

Hubei Key Laboratory for Clean Recycling and Resource Utilization of Waste Fibers, College of Chemistry and Chemical Engineering, Wuhan Textile University, Wuhan, 430200, PR China.

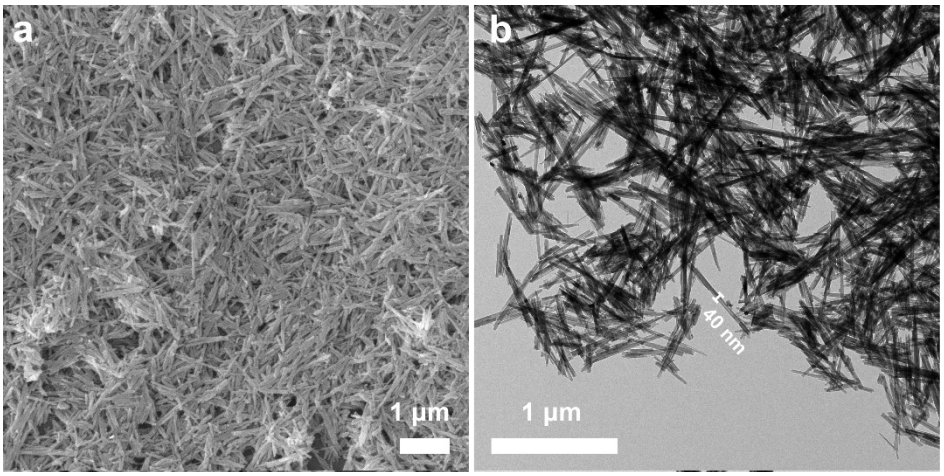

Fig. S1. Morphology and structure of α-MnO_2. (a) SEM image and (b) TEM image.

Fig. S2. Morphology and structure of β-MnO_2. (a) SEM image and (b) TEM image.

Fig. S3. Morphology and structure of γ-MnO_2. (a) SEM image and (b) TEM image.

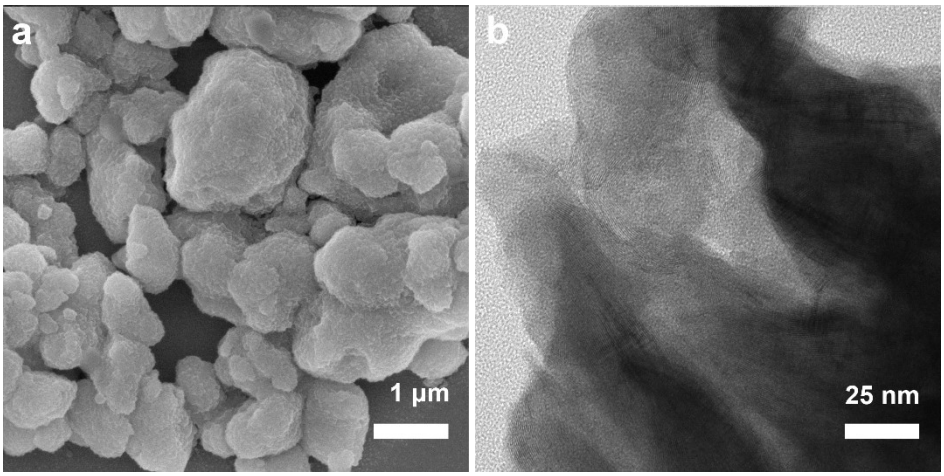

Fig. S4. Morphology and structure of δ-MnO_2. (a) SEM image and (b) TEM image.

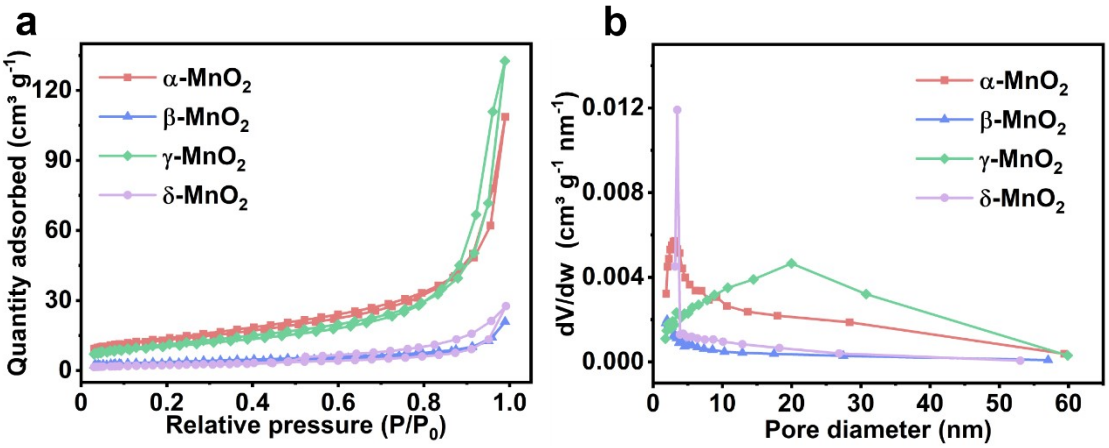

Fig. S5. (a) N_2 adsorption and desorption isotherms and (b) pore size distribution of MnO_2 polymorphs.

Table S1. BET analysis results of MnO_2 polymorphs.

	α-MnO_2	β-MnO_2	γ-MnO_2	δ-MnO_2
BET surface area (m^2/g)	50.32	13.26	41.29	8.75
Pore Volume (mL/g)	0.16	0.03	0.20	0.04

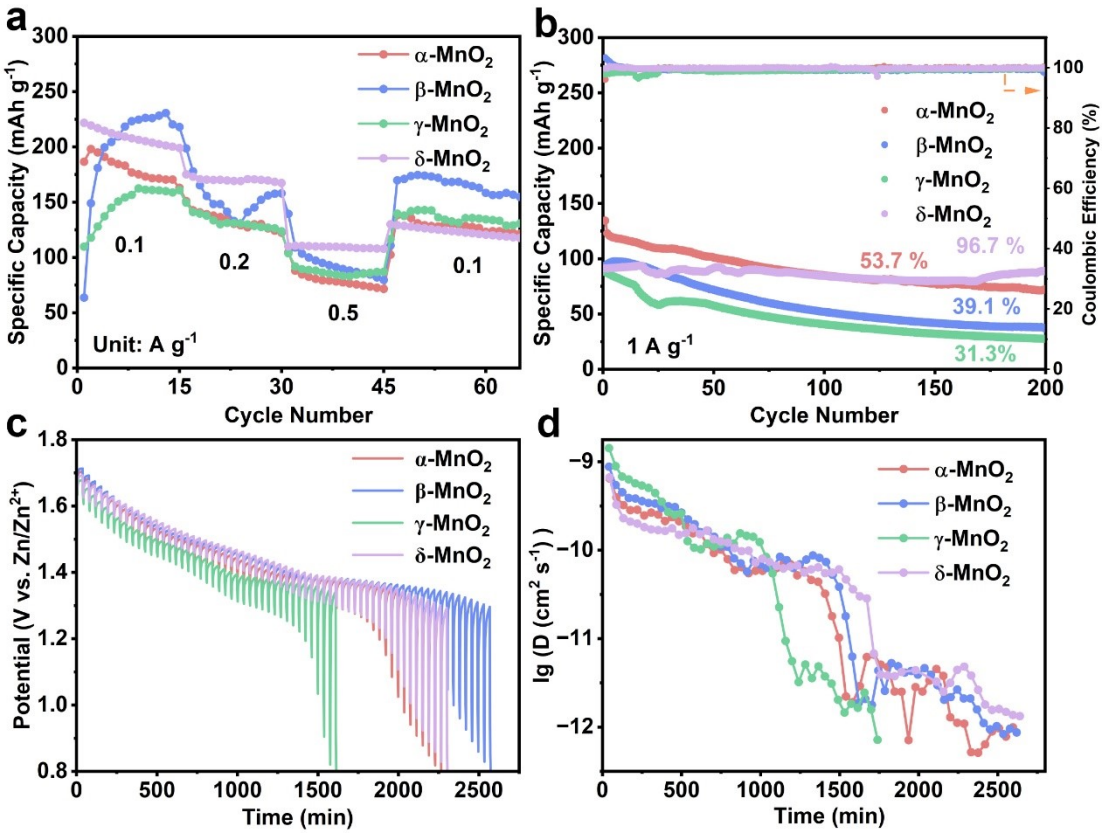

Fig. S6. Electrochemical performance and diffusion kinetics of MnO_2 polymorphs. (a) Rate performance. (b) Cycle performance at 1 A g^{-1}. (c) GITT profile. (d) The diffusion coefficient log[D/(cm^2 s^{-1})] versus discharge time.

Table S2. The average apparent diffusion coefficients of H^+ and Zn^{2+} diffusion in MnO_2 polymorphs.

Average D (10^{-11} cm^2 s^{-1})	α-MnO_2	β-MnO_2	γ-MnO_2	δ-MnO_2
H^+ diffusion	16.1	24.8	47.6	18.9
Zn^{2+} diffusion	0.24	0.26	0.17	0.31

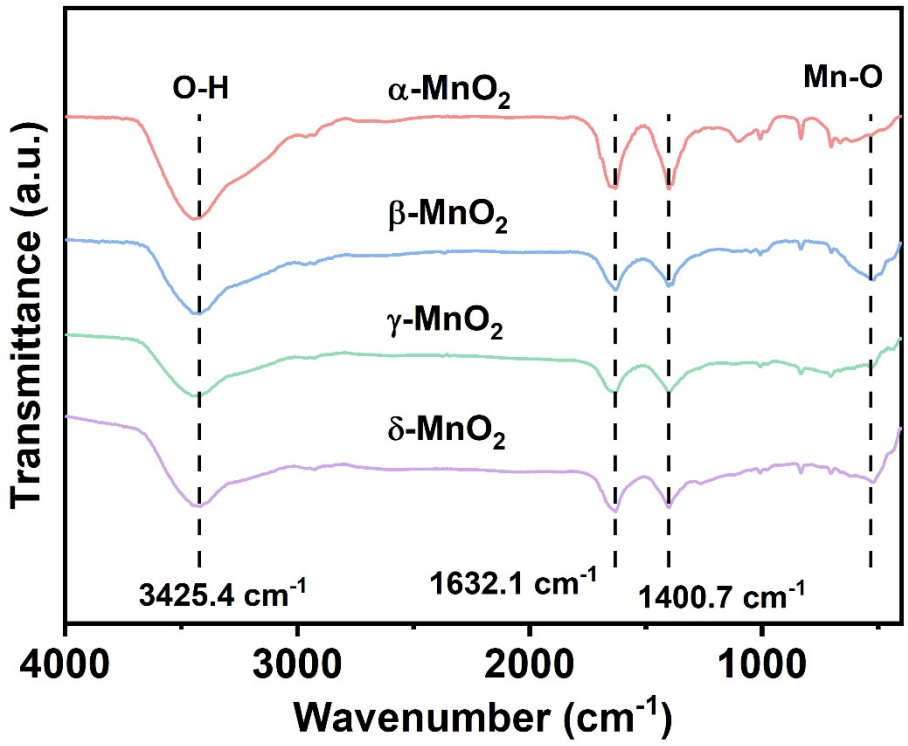

Fig. S7. FTIR of MnO_2 polymorphs.

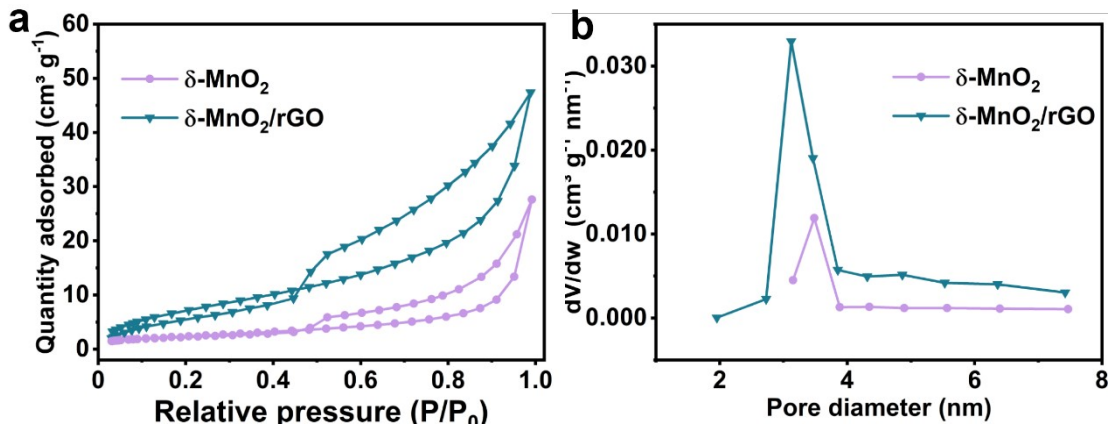

Fig. S8. (a) N_2 adsorption and desorption isotherms and (b) pore size distribution of δ-MnO_2 and δ-MnO_2/rGO.

Table S3. BET analysis results of δ-MnO_2 and δ-MnO_2/rGO.

	δ-MnO_2	δ-MnO_2/rGO
BET surface area (m^2/g)	8.75	28.94
Pore Volume (mL/g)	0.04	0.07

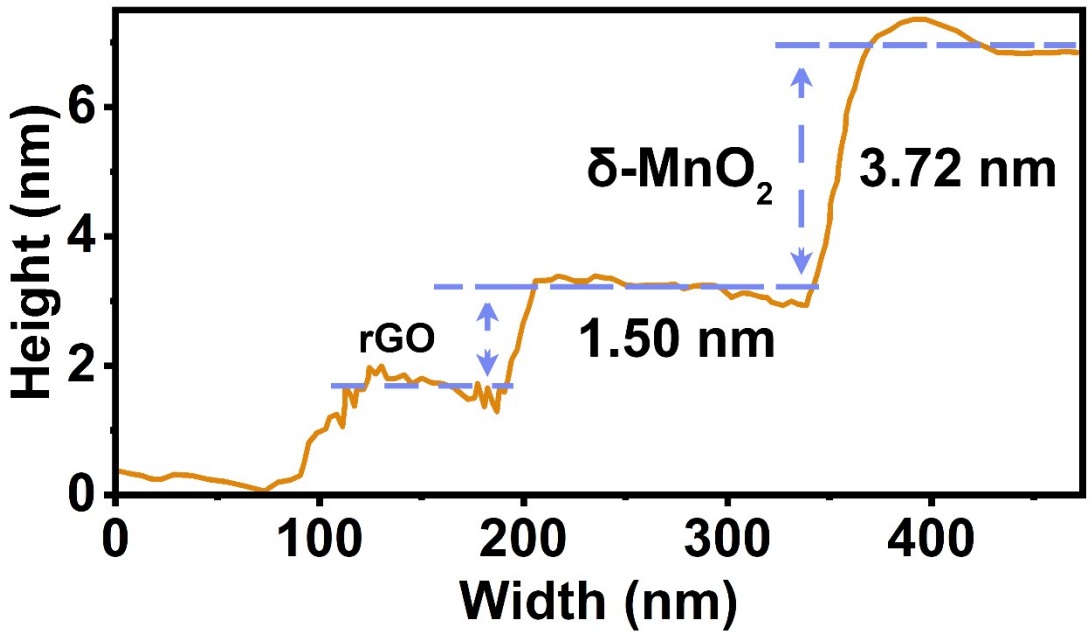

Fig. S9. Corresponding height profile of δ-MnO_2/rGO.

Fig. S10. 3D AFM image of δ-MnO_2/rGO

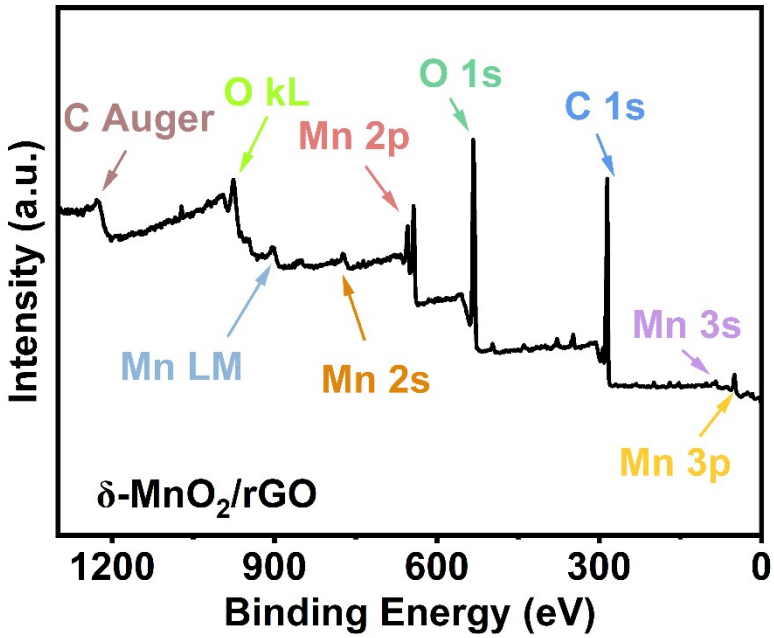

Fig. S11. XPS full spectrum of δ-MnO_2/rGO.

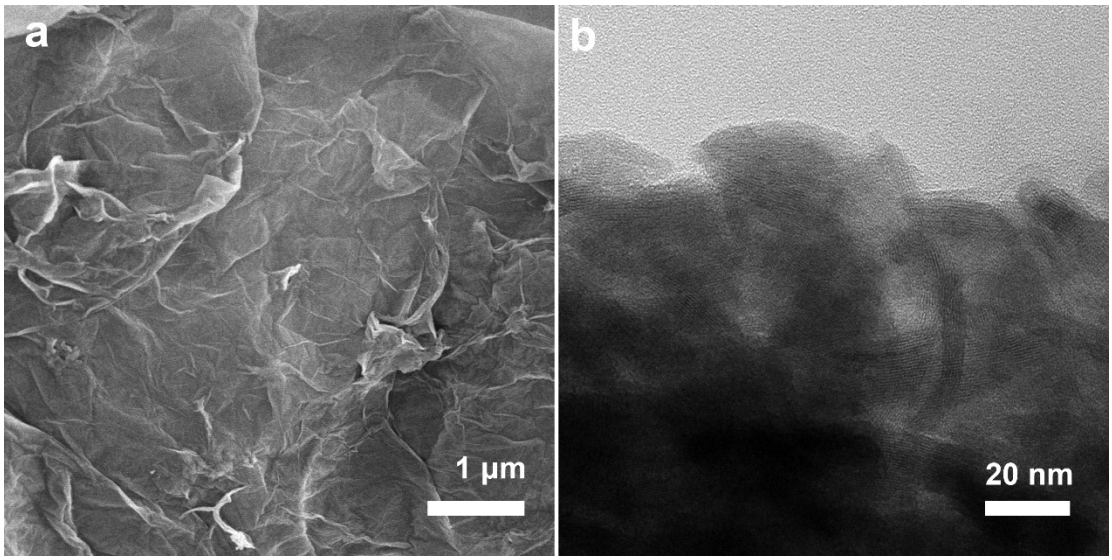

Fig. S12. (a) SEM image and (b) TEM image of δ-MnO_2/rGO.

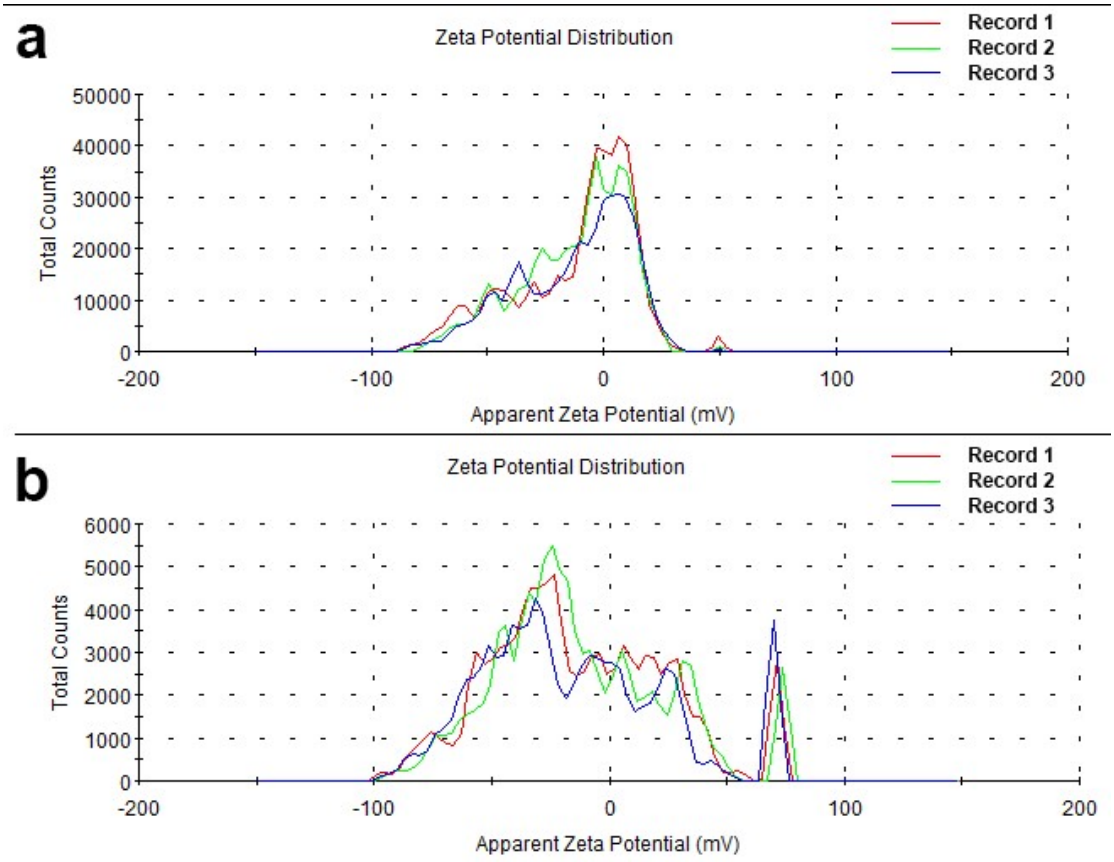

Fig. S13. Zeta Potential Distributions of (a) δ-MnO_2 and (b) rGO.

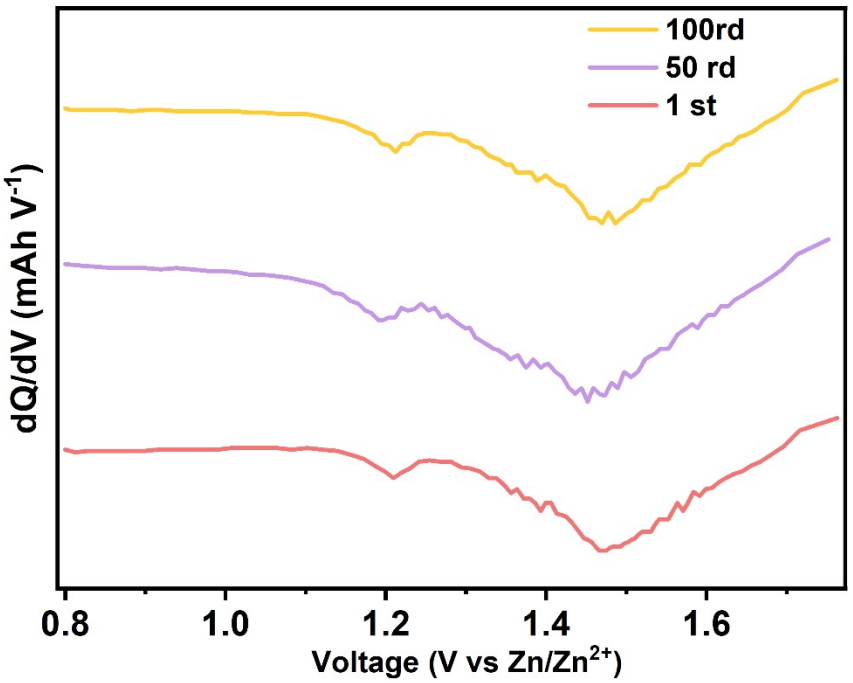

Fig. S14. dQ/dV plots of δ-MnO_2/rGO electrode.

Table S4. Summary table of contributions of H^+ and Zn^{2+}.

Cycle	Q_{Zn}^{2+} (mAh)	Q_{H}^{+} (mAh)	Zn^{2+} ratio (%)	H^+ ratio (%)
1 st	0.04	0.24	14.28	85.72
50 th	0.06	0.30	16.67	83.33
100 th	0.05	0.26	16.13	83.87
Average			15.69	84.31

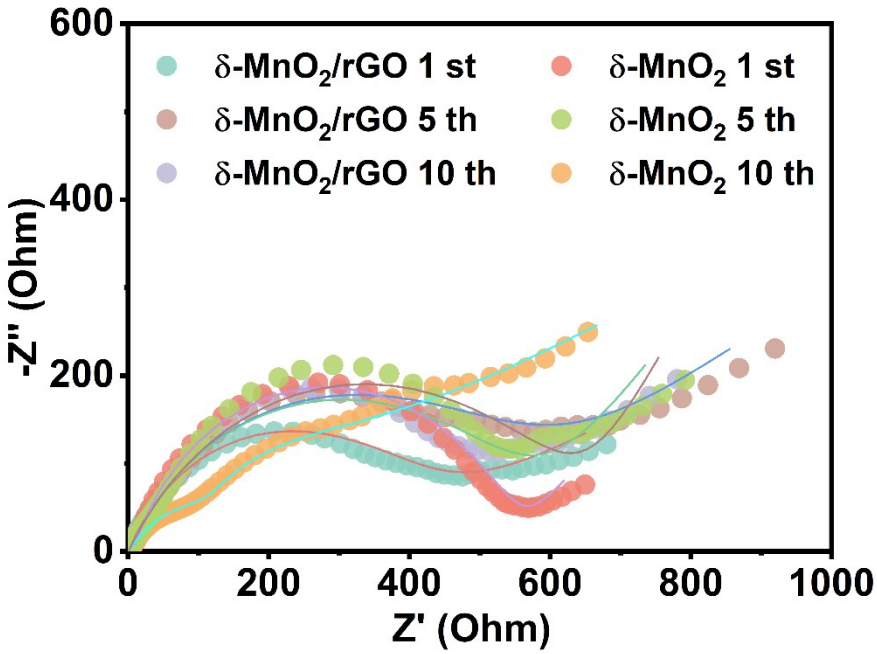

Fig. S15. EIS spectra of δ-MnO_2/rGO and δ-MnO_2 electrodes at 1^{st}–10^{th} cycles.

Table S5. EIS analysis results of δ-MnO_2 and δ-MnO_2/rGO.

Rct	δ-MnO_2	δ-MnO_2/rGO
1 st	543.33	360.96
5 th	655.4	530.38
10 th	1356.3	574.31

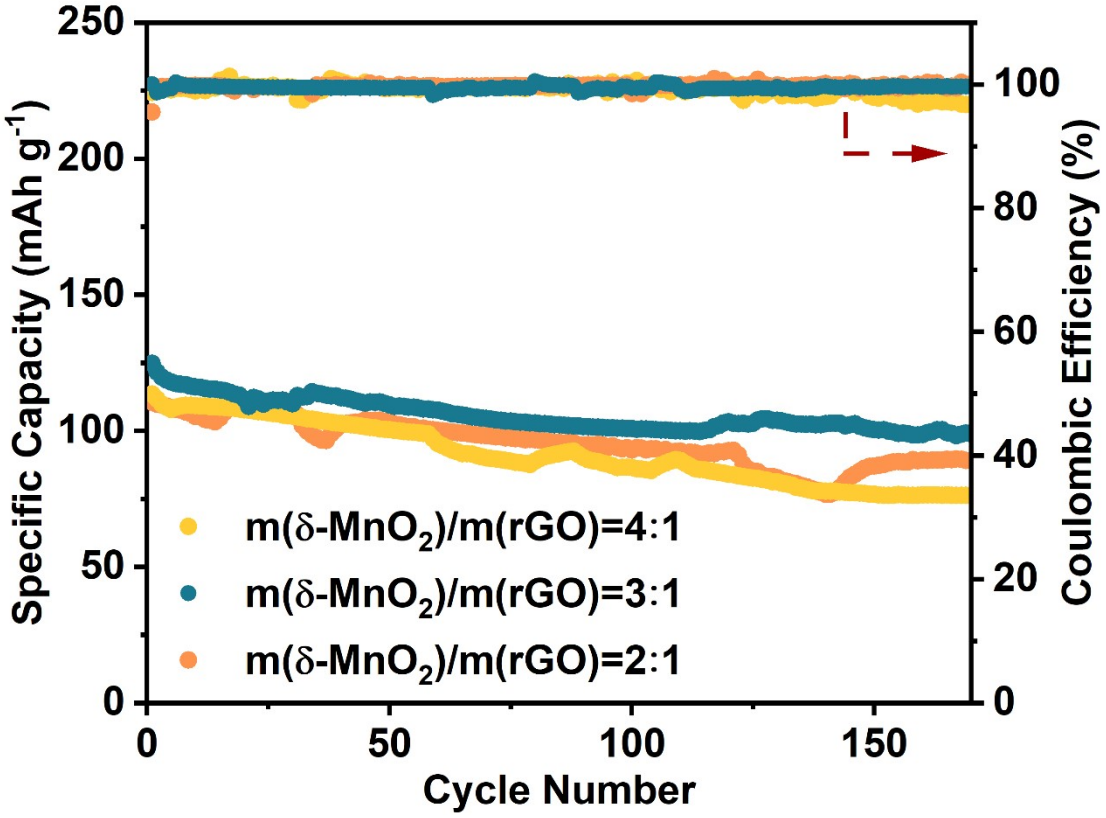

Fig. S16. Cycle performance of the δ-MnO_2/rGO electrodes with different mass ratios at current density of 1 A g^{-1}.

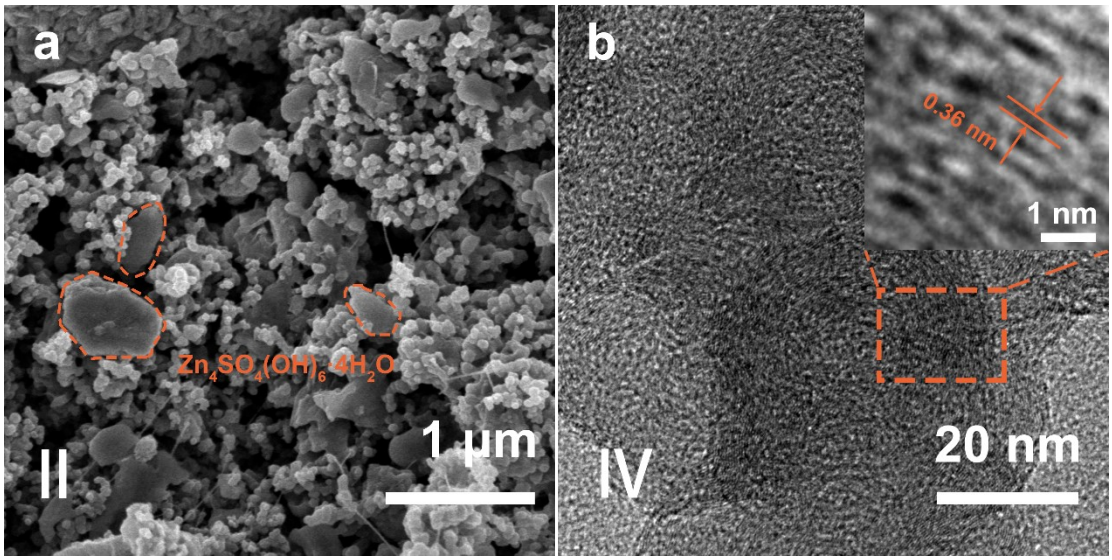

Fig. S17. (a) SEM image of II. (b) TEM image of IV.

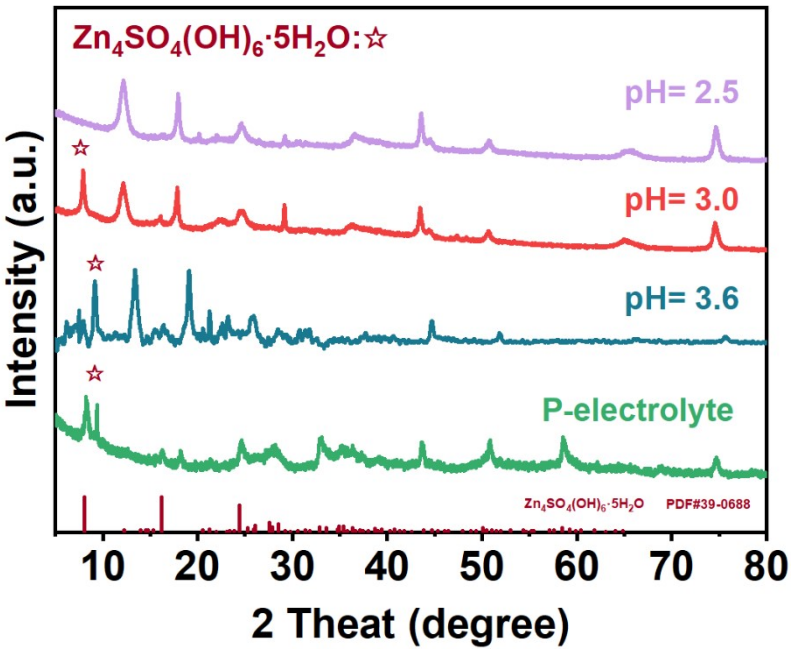

Fig. S18. XRD patterns after discharging to 0.8 V in electrolytes with different pH values.